Measurements of the branching fractions for $D^+ \to K_S^0 K_S^0 K^+$, $K_S^0 K_S^0 \pi^+$ and $D^0 \to K_S^0 K_S^0$, $K_S^0 K_S^0 K_S^0$

BESIII Collaboration

M. Ablikim [a], M.N. Achasov [i,5], S. Ahmed [n], X.C. Ai [a], O. Albayrak [e], M. Albrecht [d], D.J. Ambrose [aw], A. Amoroso [bb,bd], F.F. An [a], Q. An [ay,1], J.Z. Bai [a], R. Baldini Ferroli [t], Y. Ban [ag], D.W. Bennett [s], J.V. Bennett [e], N. Berger [x], M. Bertani [t], D. Bettoni [v], J.M. Bian [av], F. Bianchi [bb,bd], E. Boger [y,3], I. Boyko [y], R.A. Briere [e], H. Cai [bf], X. Cai [a,1], O. Cakir [ap], A. Calcaterra [t], G.F. Cao [a], S.A. Cetin [aq], J. Chai [bd], J.F. Chang [a,1], G. Chelkov [y,3,4], G. Chen [a], H.S. Chen [a], J.C. Chen [a], M.L. Chen [a,1], S. Chen [at], S.J. Chen [ae], X. Chen [a,1], X.R. Chen [ab], Y.B. Chen [a,1], H.P. Cheng [q], X.K. Chu [ag], G. Cibinetto [v], H.L. Dai [a,1], J.P. Dai [aj], A. Dbeyssi [n], D. Dedovich [y], Z.Y. Deng [a], A. Denig [x], I. Denysenko [y], M. Destefanis [bb,bd], F. De Mori [bb,bd], Y. Ding [ac], C. Dong [af], J. Dong [a,1], L.Y. Dong [a], M.Y. Dong [a,1], Z.L. Dou [ae], S.X. Du [bh], P.F. Duan [a], J.Z. Fan [ao], J. Fang [a,1], S.S. Fang [a], X. Fang [ay,1], Y. Fang [a], R. Farinelli [v,w], L. Fava [bc,bd], O. Fedorov [y], F. Feldbauer [x], G. Felici [t], C.Q. Feng [ay,1], E. Fioravanti [v], M. Fritsch [n,x], C.D. Fu [a], Q. Gao [a], X.L. Gao [ay,1], Y. Gao [ao], Z. Gao [ay,1], I. Garzia [v], K. Goetzen [j], L. Gong [af], W.X. Gong [a,1], W. Gradl [x], M. Greco [bb,bd], M.H. Gu [a,1], Y.T. Gu [l], Y.H. Guan [a], A.Q. Guo [a], L.B. Guo [ad], R.P. Guo [a], Y. Guo [a], Y.P. Guo [x], Z. Haddadi [aa], A. Hafner [x], S. Han [bf], X.Q. Hao [o], F.A. Harris [au], K.L. He [a], F.H. Heinsius [d], T. Held [d], Y.K. Heng [a,1], T. Holtmann [d], Z.L. Hou [a], C. Hu [ad], H.M. Hu [a], J.F. Hu [bb,bd], T. Hu [a,1], Y. Hu [a], G.S. Huang [ay,1], J.S. Huang [o], X.T. Huang [ai], X.Z. Huang [ae], Y. Huang [ae], Z.L. Huang [ac], T. Hussain [ba], Q. Ji [a], Q.P. Ji [o], X.B. Ji [a], X.L. Ji [a,1], L.W. Jiang [bf], X.S. Jiang [a,1], X.Y. Jiang [af], J.B. Jiao [ai], Z. Jiao [q], D.P. Jin [a,1], S. Jin [a], T. Johansson [be], A. Julin [av], N. Kalantar-Nayestanaki [aa], X.L. Kang [a], X.S. Kang [af], M. Kavatsyuk [aa], B.C. Ke [e], P. Kiese [x], R. Kliemt [n], B. Kloss [x], O.B. Kolcu [aq,8], B. Kopf [d], M. Kornicer [au], A. Kupsc [be], W. Kühn [z], J.S. Lange [z], M. Lara [s], P. Larin [n], H. Leithoff [x], C. Leng [bd], C. Li [be], Cheng Li [ay,1], D.M. Li [bh], F. Li [a,1], F.Y. Li [ag], G. Li [a], H.B. Li [a], H.J. Li [a], J.C. Li [a], Jin Li [ah], K. Li [m], K. Li [ai], Lei Li [c], P.R. Li [at], Q.Y. Li [ai], T. Li [ai], W.D. Li [a], W.G. Li [a], X.L. Li [ai], X.N. Li [a,1], X.Q. Li [af], Y.B. Li [b], Z.B. Li [an], H. Liang [ay,1], Y.F. Liang [al], Y.T. Liang [z], G.R. Liao [k], D.X. Lin [n], B. Liu [aj], B.J. Liu [a], C.X. Liu [a], D. Liu [ay,1], F.H. Liu [ak], Fang Liu [a], Feng Liu [f], H.B. Liu [l], H.H. Liu [p], H.H. Liu [a], H.M. Liu [a], J. Liu [a], J.B. Liu [ay,1], J.P. Liu [bf], J.Y. Liu [a], K. Liu [ao], K.Y. Liu [ac], L.D. Liu [ag], P.L. Liu [a,1], Q. Liu [at], S.B. Liu [ay,1], X. Liu [ab], Y.B. Liu [af], Y.Y. Liu [af], Z.A. Liu [a,1], Zhiqing Liu [x], H. Loehner [aa], X.C. Lou [a,1,7], H.J. Lu [q], J.G. Lu [a,1], Y. Lu [a], Y.P. Lu [a,1], C.L. Luo [ad], M.X. Luo [bg], T. Luo [au], X.L. Luo [a,1], X.R. Lyu [at], F.C. Ma [ac], H.L. Ma [a], L.L. Ma [ai], M.M. Ma [a], Q.M. Ma [a], T. Ma [a], X.N. Ma [af], X.Y. Ma [a,1], Y.M. Ma [ai], F.E. Maas [n], M. Maggiora [bb,bd], Q.A. Malik [ba], Y.J. Mao [ag], Z.P. Mao [a], S. Marcello [bb,bd], J.G. Messchendorp [aa], G. Mezzadri [w], J. Min [a,1], R.E. Mitchell [s], X.H. Mo [a,1], Y.J. Mo [f], C. Morales Morales [n], N.Yu. Muchnoi [i,5], H. Muramatsu [av], P. Musiol [d], Y. Nefedov [y], F. Nerling [n], I.B. Nikolaev [i,5], Z. Ning [a,1], S. Nisar [h], S.L. Niu [a,1], X.Y. Niu [a], S.L. Olsen [ah], Q. Ouyang [a,1], S. Pacetti [u], Y. Pan [ay,1], P. Patteri [t], M. Pelizaeus [d], H.P. Peng [ay,1], K. Peters [j,9], J. Pettersson [be], J.L. Ping [ad], R.G. Ping [a], R. Poling [av], V. Prasad [a], H.R. Qi [b], M. Qi [ae],

S. Qian [a,1], C.F. Qiao [at], L.Q. Qin [ai], N. Qin [bf], X.S. Qin [a], Z.H. Qin [a,1], J.F. Qiu [a], K.H. Rashid [ba], C.F. Redmer [x], M. Ripka [x], G. Rong [a], Ch. Rosner [n], X.D. Ruan [l], A. Sarantsev [y,6], M. Savrié [w], C. Schnier [d], K. Schoenning [be], S. Schumann [x], W. Shan [ag], M. Shao [ay,1], C.P. Shen [b], P.X. Shen [af], X.Y. Shen [a], H.Y. Sheng [a], M. Shi [a], W.M. Song [a], X.Y. Song [a], S. Sosio [bb,bd], S. Spataro [bb,bd], G.X. Sun [a], J.F. Sun [o], S.S. Sun [a], X.H. Sun [a], Y.J. Sun [ay,1], Y.Z. Sun [a], Z.J. Sun [a,1], Z.T. Sun [s], C.J. Tang [al], X. Tang [a], I. Tapan [ar], E.H. Thorndike [aw], M. Tiemens [aa], I. Uman [as], G.S. Varner [au], B. Wang [af], B.L. Wang [at], D. Wang [ag], D.Y. Wang [ag], K. Wang [a,1], L.L. Wang [a], L.S. Wang [a], M. Wang [ai], P. Wang [a], P.L. Wang [a], S.G. Wang [ag], W. Wang [a,1], W.P. Wang [ay,1], X.F. Wang [ao], Y. Wang [am,*], Y.D. Wang [n], Y.F. Wang [a,1], Y.Q. Wang [x], Z. Wang [a,1], Z.G. Wang [a,1], Z.H. Wang [ay,1], Z.Y. Wang [a], Z.Y. Wang [a], T. Weber [x], D.H. Wei [k], J.B. Wei [ag], P. Weidenkaff [x], S.P. Wen [a], U. Wiedner [d], M. Wolke [be], L.H. Wu [a], L.J. Wu [a], Z. Wu [a,1], L. Xia [ay,1], L.G. Xia [ao], Y. Xia [r], D. Xiao [a], H. Xiao [az], Z.J. Xiao [ad], Y.G. Xie [a,1], Q.L. Xiu [a,1], G.F. Xu [a], J.J. Xu [a], L. Xu [a], Q.J. Xu [m], Q.N. Xu [at], X.P. Xu [am], L. Yan [bb,bd], W.B. Yan [ay,1], W.C. Yan [ay,1], Y.H. Yan [r], H.J. Yang [aj], H.X. Yang [a], L. Yang [bf], Y.X. Yang [k], M. Ye [a,1], M.H. Ye [g], J.H. Yin [a], B.X. Yu [a,1], C.X. Yu [af], J.S. Yu [ab], C.Z. Yuan [a], W.L. Yuan [ae], Y. Yuan [a], A. Yuncu [aq,2], A.A. Zafar [ba], A. Zallo [t], Y. Zeng [r], Z. Zeng [ay,1], B.X. Zhang [a], B.Y. Zhang [a,1], C. Zhang [ae], C.C. Zhang [a], D.H. Zhang [a], H.H. Zhang [an], H.Y. Zhang [a,1], J. Zhang [a], J.J. Zhang [a], J.L. Zhang [a], J.Q. Zhang [a], J.W. Zhang [a,1], J.Y. Zhang [a], J.Z. Zhang [a], K. Zhang [a], L. Zhang [a], S.Q. Zhang [af], X.Y. Zhang [ai], Y. Zhang [a], Y.H. Zhang [a,1], Y.N. Zhang [at], Y.T. Zhang [ay,1], Yu Zhang [at], Z.H. Zhang [f], Z.P. Zhang [ay], Z.Y. Zhang [bf], G. Zhao [a], J.W. Zhao [a,1], J.Y. Zhao [a], J.Z. Zhao [a,1], Lei Zhao [ay,1], Ling Zhao [a], M.G. Zhao [af], Q. Zhao [a], Q.W. Zhao [a], S.J. Zhao [bh], T.C. Zhao [a], Y.B. Zhao [a,1], Z.G. Zhao [ay,1], A. Zhemchugov [y,3], B. Zheng [az], J.P. Zheng [a,1], W.J. Zheng [ai], Y.H. Zheng [at], B. Zhong [ad], L. Zhou [a,1], X. Zhou [bf], X.K. Zhou [ay,1], X.R. Zhou [ay,1], X.Y. Zhou [a], K. Zhu [a], K.J. Zhu [a,1], S. Zhu [a], S.H. Zhu [ax], X.L. Zhu [ao], Y.C. Zhu [ay,1], Y.S. Zhu [a], Z.A. Zhu [a], J. Zhuang [a,1], L. Zotti [bb,bd], B.S. Zou [a], J.H. Zou [a]

[a] *Institute of High Energy Physics, Beijing 100049, People's Republic of China*
[b] *Beihang University, Beijing 100191, People's Republic of China*
[c] *Beijing Institute of Petrochemical Technology, Beijing 102617, People's Republic of China*
[d] *Bochum Ruhr-University, D-44780 Bochum, Germany*
[e] *Carnegie Mellon University, Pittsburgh, PA 15213, USA*
[f] *Central China Normal University, Wuhan 430079, People's Republic of China*
[g] *China Center of Advanced Science and Technology, Beijing 100190, People's Republic of China*
[h] *COMSATS Institute of Information Technology, Lahore, Defence Road, Off Raiwind Road, 54000 Lahore, Pakistan*
[i] *G.I. Budker Institute of Nuclear Physics SB RAS (BINP), Novosibirsk 630090, Russia*
[j] *GSI Helmholtzcentre for Heavy Ion Research GmbH, D-64291 Darmstadt, Germany*
[k] *Guangxi Normal University, Guilin 541004, People's Republic of China*
[l] *GuangXi University, Nanning 530004, People's Republic of China*
[m] *Hangzhou Normal University, Hangzhou 310036, People's Republic of China*
[n] *Helmholtz Institute Mainz, Johann-Joachim-Becher-Weg 45, D-55099 Mainz, Germany*
[o] *Henan Normal University, Xinxiang 453007, People's Republic of China*
[p] *Henan University of Science and Technology, Luoyang 471003, People's Republic of China*
[q] *Huangshan College, Huangshan 245000, People's Republic of China*
[r] *Hunan University, Changsha 410082, People's Republic of China*
[s] *Indiana University, Bloomington, IN 47405, USA*
[t] *INFN Laboratori Nazionali di Frascati, I-00044, Frascati, Italy*
[u] *INFN and University of Perugia, I-06100, Perugia, Italy*
[v] *INFN Sezione di Ferrara, I-44122, Ferrara, Italy*
[w] *University of Ferrara, I-44122, Ferrara, Italy*
[x] *Johannes Gutenberg University of Mainz, Johann-Joachim-Becher-Weg 45, D-55099 Mainz, Germany*
[y] *Joint Institute for Nuclear Research, 141980 Dubna, Moscow region, Russia*
[z] *Justus-Liebig-Universitaet Giessen, II. Physikalisches Institut, Heinrich-Buff-Ring 16, D-35392 Giessen, Germany*
[aa] *KVI-CART, University of Groningen, NL-9747 AA Groningen, The Netherlands*
[ab] *Lanzhou University, Lanzhou 730000, People's Republic of China*
[ac] *Liaoning University, Shenyang 110036, People's Republic of China*
[ad] *Nanjing Normal University, Nanjing 210023, People's Republic of China*
[ae] *Nanjing University, Nanjing 210093, People's Republic of China*
[af] *Nankai University, Tianjin 300071, People's Republic of China*
[ag] *Peking University, Beijing 100871, People's Republic of China*
[ah] *Seoul National University, Seoul, 151-747 Republic of Korea*
[ai] *Shandong University, Jinan 250100, People's Republic of China*
[aj] *Shanghai Jiao Tong University, Shanghai 200240, People's Republic of China*
[ak] *Shanxi University, Taiyuan 030006, People's Republic of China*
[al] *Sichuan University, Chengdu 610064, People's Republic of China*
[am] *Soochow University, Suzhou 215006, People's Republic of China*
[an] *Sun Yat-Sen University, Guangzhou 510275, People's Republic of China*

ao *Tsinghua University, Beijing 100084, People's Republic of China*
ap *Ankara University, 06100 Tandogan, Ankara, Turkey*
aq *Istanbul Bilgi University, 34060 Eyup, Istanbul, Turkey*
ar *Uludag University, 16059 Bursa, Turkey*
as *Near East University, Nicosia, North Cyprus, Mersin 10, Turkey*
at *University of Chinese Academy of Sciences, Beijing 100049, People's Republic of China*
au *University of Hawaii, Honolulu, HI 96822, USA*
av *University of Minnesota, Minneapolis, MN 55455, USA*
aw *University of Rochester, Rochester, NY 14627, USA*
ax *University of Science and Technology Liaoning, Anshan 114051, People's Republic of China*
ay *University of Science and Technology of China, Hefei 230026, People's Republic of China*
az *University of South China, Hengyang 421001, People's Republic of China*
ba *University of the Punjab, Lahore-54590, Pakistan*
bb *University of Turin, I-10125, Turin, Italy*
bc *University of Eastern Piedmont, I-15121, Alessandria, Italy*
bd *INFN, I-10125, Turin, Italy*
be *Uppsala University, Box 516, SE-75120 Uppsala, Sweden*
bf *Wuhan University, Wuhan 430072, People's Republic of China*
bg *Zhejiang University, Hangzhou 310027, People's Republic of China*
bh *Zhengzhou University, Zhengzhou 450001, People's Republic of China*

A R T I C L E   I N F O

A B S T R A C T

By analyzing 2.93 fb^{-1} of data taken at the $\psi(3770)$ resonance peak with the BESIII detector, we measure the branching fractions for the hadronic decays $D^+ \to K^0_S K^0_S K^+$, $D^+ \to K^0_S K^0_S \pi^+$, $D^0 \to K^0_S K^0_S$ and $D^0 \to K^0_S K^0_S K^0_S$. They are determined to be $\mathcal{B}(D^+ \to K^0_S K^0_S K^+) = (2.54 \pm 0.05_{\text{stat.}} \pm 0.12_{\text{sys.}}) \times 10^{-3}$, $\mathcal{B}(D^+ \to K^0_S K^0_S \pi^+) = (2.70 \pm 0.05_{\text{stat.}} \pm 0.12_{\text{sys.}}) \times 10^{-3}$, $\mathcal{B}(D^0 \to K^0_S K^0_S) = (1.67 \pm 0.11_{\text{stat.}} \pm 0.11_{\text{sys.}}) \times 10^{-4}$ and $\mathcal{B}(D^0 \to K^0_S K^0_S K^0_S) = (7.21 \pm 0.33_{\text{stat.}} \pm 0.44_{\text{sys.}}) \times 10^{-4}$, where the second one is measured for the first time and the others are measured with significantly improved precision over the previous measurements.

© 2016 The Author(s). Published by Elsevier B.V. This is an open access article under the CC BY license (http://creativecommons.org/licenses/by/4.0/). Funded by SCOAP^3.

1. Introduction

Hadronic decays of D mesons open a window to probe for the physics mechanisms in charmed meson decays, *e.g.*, CP violation, $D^0 \bar{D}^0$ mixing and SU(3) symmetry breaking effects. Since the discovery of D mesons in 1976, the hadronic decays of D mesons have been extensively investigated [1]. However, the existing measurements of the D hadronic decays containing at least two K^0_S mesons in the final state are still very poor due to limited statistics [1].

In this Letter, we report the measurements of the branching fractions for the hadronic decays $D^+ \to K^0_S K^0_S \pi^+$, $D^0 \to K^0_S K^0_S$, $D^+ \to K^0_S K^0_S K^+$ and $D^0 \to K^0_S K^0_S K^0_S$. Throughout this Letter, charged conjugate modes are implied. These decays have simpler event topologies and suffer less from combinatorial backgrounds than other decay modes containing two K^0_S in the final state. The comprehensive or improved measurements of three-body decays will benefit the understanding of the interplay between the weak and strong interactions in multibody decays where theoretical predictions are poorer than two-body decays. The improved measurements of two-body decays can serve to better explore the contributions of W-exchange diagrams and final-state interactions [2–5], as well as SU(3)-flavor symmetry breaking effects [6–10] in D meson decays. In addition, these measurements will also help to improve background estimations in the precision measurements of D and B meson decays.

The data sample used for this analysis, which has an integrated luminosity of 2.93 fb^{-1} [11], was taken at the $\psi(3770)$ resonance peak with the BESIII detector [12]. The $D^0 \bar{D}^0$ and $D^+ D^-$ pairs produced in $\psi(3770)$ decay provide cleaner D^0 and D^+ meson samples than those used in previous studies at ARGUS [13,14], CLEO [15,16] and FOCUS [17]. To optimize the precision for these measurements, we use a single-tag method, in which either a D or $\bar{D}$ is reconstructed in an event. We combine the yields measured with previously reported values of the cross sections for $e^+ e^- \to D^0 \bar{D}^0$ and $D^+ D^-$ at the $\psi(3770)$ resonance peak [18].

2. BESIII detector and Monte Carlo simulation

The BESIII detector is a magnetic spectrometer that operates at the BEPCII collider. It has a cylindrical geometry with a solid-angle coverage of 93% of 4π. It consists of several main components. A 43-layer main drift chamber (MDC) surrounding the beam pipe performs precise determinations of charged particle trajectories and measures the specific ionization (dE/dx) for charged particle identification (PID). An array of time-of-flight counters (TOF) is located outside the MDC and provides additional PID information. A CsI(Tl) electromagnetic calorimeter (EMC) surrounds the TOF and is used to measure the energies of photons and electrons. A solenoidal superconducting magnet outside the EMC provides a 1 T magnetic field in the central tracking region of the detector.

* Corresponding author.
E-mail address: wangyue0108@ihep.ac.cn (Y. Wang).
1 Also at State Key Laboratory of Particle Detection and Electronics, Beijing 100049, Hefei 230026, People's Republic of China.
2 Also at Bogazici University, 34342 Istanbul, Turkey.
3 Also at the Moscow Institute of Physics and Technology, Moscow 141700, Russia.
4 Also at the Functional Electronics Laboratory, Tomsk State University, Tomsk, 634050, Russia.
5 Also at the Novosibirsk State University, Novosibirsk, 630090, Russia.
6 Also at the NRC "Kurchatov Institute", PNPI, 188300, Gatchina, Russia.
7 Also at the University of Texas at Dallas, Richardson, TX 75083, USA.
8 Also at Istanbul Arel University, 34295 Istanbul, Turkey.
9 Also at Goethe University Frankfurt, 60323 Frankfurt am Main, Germany.
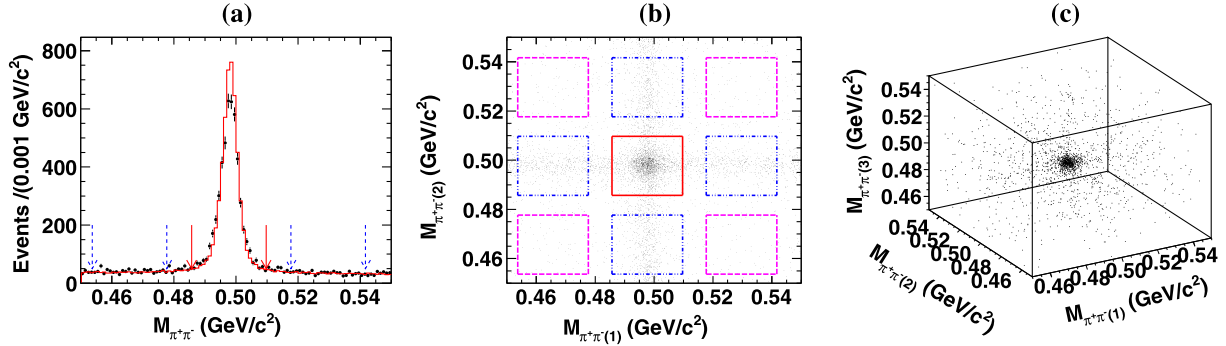
Fig. 1. (a) Comparison of the $M_{\pi^+\pi^-}$ distributions of the $D^0 \to K_S^0 K_S^0$ candidate events between data (dots with error bars) and inclusive MC (histogram). The pairs of the solid (dashed) arrows denote the K_S^0 signal (sideband) regions. (b) Distribution of $M_{\pi^+\pi^-(1)}$ versus $M_{\pi^+\pi^-(2)}$ for the $D^0 \to K_S^0 K_S^0$ candidate events in data. (c) Distribution of $M_{\pi^+\pi^-(1)}$ versus $M_{\pi^+\pi^-(2)}$ versus $M_{\pi^+\pi^-(3)}$ for the $D^0 \to K_S^0 K_S^0 K_S^0$ candidate events in data. In these figures, all selection criteria have been imposed except for the K_S^0 mass requirement and M_{BC} is required to be within 5 MeV/c^2 around the D nominal mass [1].

The iron flux return of the magnet is instrumented with 1272 m^2 of resistive plate muon counters (MUC) arranged in nine layers in the barrel and eight layers in the endcaps for identification of muons with momentum greater than 0.5 GeV/c. More details about the BESIII detector are described in Ref. [12].

A GEANT4-based [19] Monte Carlo (MC) simulation software package, which includes the geometric description and response of the detector, is used to determine the detection efficiency and to estimate background for each decay mode. An inclusive MC sample, which includes the $D^0 \bar{D}^0$, $D^+ D^-$ and non-$D\bar{D}$ decays of the $\psi(3770)$, initial-state-radiation (ISR) production of the $\psi(3686)$ and J/ψ, the $e^+ e^- \to q\bar{q}$ ($q = u, d, s$) continuum process, the Bhabha scattering events, the di-muon events and the di-tau events, is produced at $\sqrt{s} = 3.773$ GeV. The equivalent luminosity of the MC sample is ten times of data. The $\psi(3770)$ decays are generated by the MC generator KKMC [20], which incorporates both ISR effects [21] and final-state-radiation (FSR) effects [22]. Known decay modes are generated using EvtGen [23] with input branching fractions from the Particle Data Group (PDG) [1]. Unmeasured decays are generated using LundCharm [24].

3. Data analysis

All charged tracks used in this analysis are required to be within a polar-angle (θ) range of $|\cos\theta| < 0.93$. The good charged tracks, except when used to reconstruct K_S^0 mesons, are required to originate within an interaction region defined by $V_{xy} < 1.0$ cm and $V_z < 10.0$ cm, where V_{xy} and V_z are the distances of closest approach of the reconstructed track to the interaction point (IP) perpendicular to (xy) and along (z) the beam direction.

The charged kaons and pions are identified by the dE/dx and TOF measurements. The combined confidence levels for pion and kaon hypotheses (CL_π and CL_K) are calculated, respectively. The charged track is identified as kaon (pion) if $CL_K > CL_\pi$ ($CL_\pi > CL_K$) is satisfied.

K_S^0 candidate mesons are reconstructed through the $\pi^+\pi^-$ decay mode. Charged pions used in K_S^0 candidates mesons are required to satisfy $V_z < 20.0$ cm. The two oppositely charged tracks are assumed to be a $\pi^+\pi^-$ pair without PID requirements. To reconstruct K_S^0, the $\pi^+\pi^-$ combination is constrained to have a common vertex. The candidate is accepted if it has an invariant mass $M_{\pi^+\pi^-}$ within 12 MeV/c^2 of the K_S^0 nominal mass [1] and satisfies $L/\sigma_L > 2$, where L is the measured flight distance and σ_L is its uncertainty.

To identify D candidates, we use two selection variables, the energy difference $\Delta E \equiv E_{beam} - E_D$ and the beam-energy-constrained mass $M_{BC} \equiv \sqrt{E_{beam}^2/c^4 - |\vec{p}_D|^2/c^2}$, where E_{beam} is

Table 1
ΔE requirements (in MeV) for data and MC samples.

Decay modes	Data	MC
$D^+ \to K_S^0 K_S^0 K^+$	$(-17, +19)$	$(-16, +16)$
$D^+ \to K_S^0 K_S^0 \pi^+$	$(-17, +17)$	$(-17, +16)$
$D^0 \to K_S^0 K_S^0$	$(-19, +17)$	$(-17, +14)$
$D^0 \to K_S^0 K_S^0 K_S^0$	$(-14, +16)$	$(-13, +13)$

the beam energy and E_D and $\vec{p}_D$ are the energy and momentum of the D candidate in the $e^+ e^-$ center-of-mass system. For each signal decay mode, only the combination with the minimum $|\Delta E|$ is kept in events where more than one candidate passes the selection requirements. Mode-dependent ΔE cuts are determined separately for data and MC based on fits to the respective ΔE distributions. These are set at $\pm 3\sigma$, where σ is the ΔE resolution (Table 1).

The combinatorial $\pi^+\pi^-|_{non-K_S^0}$ pairs with invariant mass in K_S^0 signal region may also satisfy the K_S^0 selection criteria and contribute peaking background around the D mass in the M_{BC} distribution. This peaking background is estimated with events in the K_S^0 sideband region, defined as $0.020 < |M_{\pi^+\pi^-} - M_{K_S^0}| < 0.044$ GeV/c^2. Fig. 1(a) shows the comparison of the $M_{\pi^+\pi^-}$ distribution for $D^0 \to K_S^0 K_S^0$ candidates in data with the corresponding distribution for the inclusive MC. In the figure, the solid (dashed) arrows delineate the K_S^0 signal (sideband) regions.

In the analyses of the $D^0 \to K_S^0 K_S^0$, $D^+ \to K_S^0 K_S^0 K^+$ and $K_S^0 K_S^0 \pi^+$ decays, two-dimensional (2D) signal and sideband regions are defined. Fig. 1(b) shows the distribution of $M_{\pi^+\pi^-(1)}$ versus $M_{\pi^+\pi^-(2)}$ for the $D^0 \to K_S^0 K_S^0$ candidate events in data. The solid box, in which both of the $\pi^+\pi^-$ combinations lie in the K_S^0 signal regions, denotes the 2D signal region. The dot-dashed (dashed) boxes indicate the 2D sideband 1 (2) regions, in which one (two) of the $\pi^+\pi^-$ combinations lie in the K_S^0 sideband regions and the others are in the K_S^0 signal region. For the $D^0 \to K_S^0 K_S^0 K_S^0$ decay, $M_{\pi^+\pi^-(1)}$ versus $M_{\pi^+\pi^-(2)}$ versus $M_{\pi^+\pi^-(3)}$ of the candidate events in data is shown in Fig. 1 (c). The region in which all three $\pi^+\pi^-$ combinations lie in the K_S^0 signal regions is taken as the three-dimensional (3D) signal region. The 3D sideband i ($i = 1, 2, 3$) regions denote those in which i of the three $\pi^+\pi^-$ pairs lie in the K_S^0 sideband regions and the rest are located in the K_S^0 signal regions.

The resulting M_{BC} distributions of the accepted candidate events in the 2D or 3D signal region, sideband 1 region and sideband 2 region are shown in the sub-figures of the first, second and third rows of Fig. 2, respectively. By fitting these M_{BC} distri-
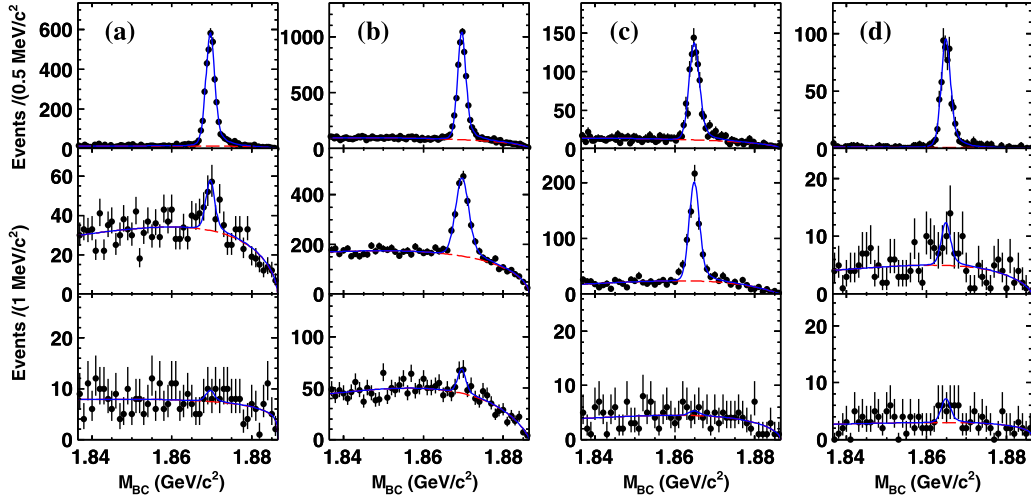
Fig. 2. Fits to the M_{BC} distributions of the (a) $D^+ \to K_S^0 K_S^0 K^+$, (b) $D^+ \to K_S^0 K_S^0 \pi^+$, (c) $D^0 \to K_S^0 K_S^0$ and (d) $D^0 \to K_S^0 K_S^0 K_S^0$ candidate events. The dots with error bars are data, the solid curves are the total fits, and the dashed curves are the fitted backgrounds. The first, second and third rows correspond to the fits to the candidate events in the 2D or 3D signal region, sideband 1 region and sideband 2 region, respectively.

Table 2
Input quantities and results for the determination of the branching fractions as described in the text. The uncertainties are statistical only.

Decay modes	$N_{K_S^0\text{sig}}$	N_{sb1}	N_{sb2}	N_{sb3}	$N_{\text{other}}^{\text{b}}$	N_{net}	ϵ (%)	$\mathcal{B}$ ($\times 10^{-4}$)
$D^+ \to K_S^0 K_S^0 K^+$	3616 ± 66	97 ± 19	6 ± 8	–	18 ± 2	3551 ± 67	8.27 ± 0.04	25.4 ± 0.5
$D^+ \to K_S^0 K_S^0 \pi^+$	5643 ± 88	1464 ± 68	69 ± 19	–	31 ± 3	4897 ± 94	10.72 ± 0.04	27.0 ± 0.5
$D^0 \to K_S^0 K_S^0$	888 ± 36	626 ± 31	3 ± 6	–	0	576 ± 39	16.28 ± 0.30	1.67 ± 0.11
$D^0 \to K_S^0 K_S^0 K_S^0$	622 ± 27	24 ± 8	14 ± 6	0	16 ± 3	597 ± 27	3.92 ± 0.05	7.21 ± 0.33

butions as shown in Fig. 2, we obtain the fitted yields of D signal in the 2D or 3D signal region, sideband 1 region and sideband 2 region, $N_{K_S^0\text{sig}}$, N_{sb1}, N_{sb2}, which are given in Table 2. In the fits, the D signal is modeled by a MC-simulated shape convoluted with a Gaussian function with free parameters accounting for the difference of detector resolution between data and MC. The combinatorial backgrounds are described by an ARGUS function [25] with an endpoint of 1.8865 GeV/c^2. In the M_{BC} fits for the 2D or 3D sideband events, the parameters of the convoluted Gaussian function are fixed at the values determined for the signal region. For the $D^0 \to K_S^0 K_S^0 K_S^0$ decays, the peaking backgrounds from sideband 3 region are negligible since few events survive.

In this analysis, the combinatorial background in the $M_{\pi^+\pi^-}$ distribution is assumed to be flat, which implies that the ratio of background yields between the K_S^0 signal and sideband regions is 0.5. Thus, the net numbers of the $D^0 \to K_S^0 K_S^0$, $D^+ \to K_S^0 K_S^0 K^+$ and $K_S^0 K_S^0 \pi^+$ decays can be calculated by

$$N_{\text{net}} = N_{K_S^0\text{sig}} - \frac{1}{2}N_{\text{sb1}} + \frac{1}{4}N_{\text{sb2}} - N_{\text{other}}^{\text{b}}, \qquad (1)$$

and the net number of the $D^0 \to K_S^0 K_S^0 K_S^0$ decays can be calculated by

$$N_{\text{net}} = N_{K_S^0\text{sig}} - \frac{1}{2}N_{\text{sb1}} + \frac{1}{4}N_{\text{sb2}} - \frac{1}{8}N_{\text{sb3}} - N_{\text{other}}^{\text{b}}, \qquad (2)$$

where $N_{K_S^0\text{sig}}$ and $N_{\text{sb}i}$ are D signal yields from the fit in the 2D or 3D signal regions and sideband i regions, respectively. $N_{\text{other}}^{\text{b}}$ is the normalized number of residual peaking background. For the $D^+ \to K_S^0 K_S^0 K^+$, $D^+ \to K_S^0 K_S^0 \pi^+$ and $D^0 \to K_S^0 K_S^0 K_S^0$ decays, the residual peaking background is mainly from the events of $D^+ \to K_S^0 K_L^0 K^+$, $D^+ \to K_S^0 K_L^0 \pi^+$ and $D^0 \to K_S^0 K_S^0 K_L^0$ versus $D^- (\bar{D}^0) \to K_S^0 X$ ($X =$ any possible particle combination). This kind of background peaks

around the nominal D mass [1] when the K_S^0 from a $D^- (\bar{D}^0)$ decay has momentum similar to that of a K_L^0 produced in $D^+ (D^0)$ decay. These peaking backgrounds cannot be modeled by the events from the 2D or 3D sideband region and are estimated by analyzing the inclusive MC sample. The measured values of $N_{\text{other}}^{\text{b}}$ and N_{net} are given in Table 2.

4. Branching fractions

The branching fraction for the hadronic decay $D^{+(0)} \to f$ is determined by

$$\mathcal{B}(D^{+(0)} \to f) = \frac{N_{\text{net}}}{2 \cdot \sigma_{D^+D^- (D^0\bar{D}^0)} \cdot \mathcal{L} \cdot \epsilon}, \qquad (3)$$

where N_{net} is the net number of $D^{+(0)} \to f$ decays in data, ϵ is the detection efficiency including the branching fraction of $K_S^0 \to \pi^+\pi^-$, $\mathcal{L}$ is the integrated luminosity of data [11] and $\sigma_{D^+D^- (D^0\bar{D}^0)}$ is the $D^+D^- (D^0\bar{D}^0)$ cross section at the $\psi(3770)$ resonance peak.

The detection efficiencies are determined by analyzing the inclusive MC sample. In this sample, the signal MC events for $D^+ \to K_S^0 K_S^0 \pi^+$ are produced as a mixed sample containing 90% of the $D^+ \to K_S^0 K^*(892)^+$, $K^*(892)^+ \to K_S^0 \pi^+$ decays and 10% of the direct three-body decay in phase space $D^+ \to K_S^0 K_S^0 \pi^+$. The signal MC events for $D^+ \to K_S^0 K_S^0 K^+$, $D^0 \to K_S^0 K_S^0$ and $K_S^0 K_S^0 K_S^0$ are produced using a phase–space model. Detailed studies show that the momentum and polar-angle distributions of the daughter particles in data are well modeled by the MC simulation for each decay mode. By analyzing the inclusive MC sample with the same analysis procedure applied to the data (including the M_{BC} fits and the calculation of the net signal yields), we obtain the net number of D mesons observed for each decay. The detection efficiency ϵ is

Table 3

Systematic uncertainties (%) in the branching fraction measurements.

Sources	$D^+ \to K_S^0 K_S^0 K^+$	$D^+ \to K_S^0 K_S^0 \pi^+$	$D^0 \to K_S^0 K_S^0$	$D^0 \to K_S^0 K_S^0 K_S^0$
MC statistics	0.5	0.4	1.8	1.3
Luminosity of data	0.5	0.5	0.5	0.5
$D\bar{D}$ cross section	1.6	1.6	1.6	1.6
$\mathcal{B}(K_S^0 \to \pi^+\pi^-)$	0.2	0.2	0.2	0.3
K_S^0 reconstruction	3.0	3.0	3.0	4.5
Tracking for $K^+(\pi^+)$	0.5	0.5	–	–
PID for $K^+(\pi^+)$	0.5	0.5	–	–
M_{BC} fit	2.1	1.0	4.2	2.7
ΔE requirement	2.0	1.5	2.0	1.5
PBKG normalization	0.5	1.4	2.4	0.8
K_S^0 sideband	0.5	0.5	2.0	1.0
MC modeling	1.0	1.0	–	1.0
Total	4.7	4.4	6.8	6.1

obtained by dividing the net D signal by the total number of signal events, taking into account the efficiency correction discussed in Sect. 5.

Inserting the numbers of N_{net}, ϵ, $\mathcal{L}$, as well as $\sigma_{D^+D^-} = (2.882 \pm 0.018_{stat.} \pm 0.042_{sys.})$ nb or $\sigma_{D^0\bar{D}^0} = (3.607 \pm 0.017_{stat.} \pm 0.056_{sys.})$ nb quoted from Ref. [18] into Eq. (3), we obtain the branching fraction for each decay, as listed in Table 2, where the uncertainties are statistical only.

5. Systematic uncertainty

Table 3 shows the systematic uncertainties in the branching fraction measurements. Each of them, estimated relative to the measured branching fraction, is discussed below.

- *MC statistics*: The uncertainties due to the limited MC statistics are 0.5%, 0.4%, 1.8% and 1.3% for $D^+ \to K_S^0 K_S^0 K^+$, $D^+ \to K_S^0 K_S^0 \pi^+$, $D^0 \to K_S^0 K_S^0$ and $D^0 \to K_S^0 K_S^0 K_S^0$, respectively.
- *Luminosity of data*: The uncertainty in the quoted integrated luminosity of data is 0.5% [11].
- *$D\bar{D}$ cross section*: The uncertainties of the quoted D^+D^- and $D^0\bar{D}^0$ cross sections are 1.6% [18].
- *$\mathcal{B}(K_S^0 \to \pi^+\pi^-)$*: The uncertainty of the quoted branching fraction for $K_S^0 \to \pi^+\pi^-$ is 0.1% [1].
- *K_S^0 reconstruction*: The K_S^0 reconstruction efficiency has been studied as a function of momentum by using the control samples $J/\psi \to K^*(892)^{\mp}K^{\pm}$ and $J/\psi \to \phi K_S^0 K^{\pm}\pi^{\mp}$. Small data-MC efficiency differences are found and presented in Ref. [26]. To correct the K_S^0 reconstruction efficiency, a piecewise fit to these differences as a function of K_S^0 momentum is performed. For the efficiencies of detecting the decays $D^+ \to K_S^0 K_S^0 K^+$, $D^+ \to K_S^0 K_S^0 \pi^+$, $D^0 \to K_S^0 K_S^0$ and $D^0 \to K_S^0 K_S^0 K_S^0$, the momentum weighted differences associated with K_S^0 reconstruction between data and MC are determined to be $(+3.9 \pm 1.9)\%$, $(+3.0 \pm 1.4)\%$, $(+1.8 \pm 0.8)\%$ and $(+5.9 \pm 2.8)\%$, respectively, where the uncertainties are statistical. These corrections are applied to the detection efficiencies, after which only the statistical uncertainties of the differences are retained. On average, the residual uncertainty for each K_S^0 is no more than 1.0%. Furthermore, the difference of the momentum-weighted efficiencies between data and MC from the different fits, which is 1.0% per K_S^0, is included as an additional uncertainty. Finally, we assign 1.5% per K_S^0 as the systematic uncertainty for the reconstruction efficiency.
- *Tracking [PID] for $K^+(\pi^+)$*: The tracking [PID] efficiencies for K^+ and π^+ are investigated using doubly tagged $D\bar{D}$ hadronic events. The difference of momentum weighted efficiencies between data and MC of the tracking [PID] are determined to

be $(+2.1 \pm 0.4)\%$ $[(-0.3 \pm 0.1)\%]$ for the K^+ in the $D^+ \to K_S^0 K_S^0 K^+$ decay and $(+0.4 \pm 0.3)\%$ $[(-0.3 \pm 0.1)\%]$ for the π^+ in the $D^+ \to K_S^0 K_S^0 \pi^+$ decay, where the uncertainties are statistical. After correcting the detection efficiencies by these differences, we take 0.5% [0.5%] as the systematic uncertainties in tracking [PID] for the K^+ and π^+, respectively.
- *M_{BC} fit*: In order to estimate the systematic uncertainty associated with the M_{BC} fit, we repeat the measurements by varying the fit range $((1.8415, 1.8865)$ GeV/$c^2)$, signal shape (with different MC matching requirements) and endpoint of the ARGUS function (± 0.2 MeV/c^2). Quadratically summing the changes of the branching fractions yields 2.1%, 1.0%, 4.2% and 2.7% for $D^+ \to K_S^0 K_S^0 K^+$, $D^+ \to K_S^0 K_S^0 \pi^+$, $D^0 \to K_S^0 K_S^0$ and $D^0 \to K_S^0 K_S^0 K_S^0$, which are assigned as the relevant systematic uncertainties.
- *ΔE requirement*: To investigate the systematic uncertainty associated with the ΔE requirement, we repeat the measurements using alternative ΔE requirements of $\pm (4, 5, 6)$ times the resolution around the ΔE peaks. The maximum changes of the branching fractions, 2.0%, 1.5%, 2.0% and 1.5% for $D^+ \to K_S^0 K_S^0 K^+$, $D^+ \to K_S^0 K_S^0 \pi^+$, $D^0 \to K_S^0 K_S^0$ and $D^0 \to K_S^0 K_S^0 K_S^0$, are taken as the associated systematic uncertainties.
- *Normalization of peaking backgrounds*: In the nominal analysis, the normalization factor for the peaking backgrounds, which is the ratio of background yields between the K_S^0 signal and sideband regions, has been assumed to be 0.5. The branching fractions are recalculated with alternative normalization factors determined by MC simulation. The corresponding changes on the branching fractions, 0.5%, 1.4%, 2.4% and 0.7% for $D^+ \to K_S^0 K_S^0 K^+$, $D^+ \to K_S^0 K_S^0 \pi^+$, $D^0 \to K_S^0 K_S^0$ and $D^0 \to K_S^0 K_S^0 K_S^0$, are assigned as the systematic uncertainties associated with the peaking background (PBKG) normalization. On the other hand, the uncertainties of the residual peaking backgrounds are dominated by the uncertainties of the input branching fractions for $D^-(\bar{D}^0) \to K_S^0 X$, which contribute additional uncertainties of 0.1%, 0.1% and 0.4% for the measured branching fractions for $D^+ \to K_S^0 K_S^0 K^+$, $D^+ \to K_S^0 K_S^0 \pi^+$ and $D^0 \to K_S^0 K_S^0 K_S^0$, respectively.
- *K_S^0 sideband*: To evaluate the systematic uncertainty due to the choice of K_S^0 sideband region, we remeasure the branching fractions after shifting the K_S^0 sideband by ± 2 MeV/c^2. The corresponding maximum changes in the branching fraction, which are 0.5%, 0.5%, 2.0% and 1.0% for $D^+ \to K_S^0 K_S^0 K^+$, $D^+ \to K_S^0 K_S^0 \pi^+$, $D^0 \to K_S^0 K_S^0$ and $D^0 \to K_S^0 K_S^0 K_S^0$, respectively, are taken as the systematic uncertainties.
- *MC modeling*: For the three-body decays, we examine the reweighted detection efficiencies by including the possible sub-resonances $a_0(980)$ and $f_0(980)$ in the signal MC samples.

Table 4
Comparisons of the branching fractions (in 10^{-4}) measured in this work with the PDG values [1].

Decay modes	This work	PDG
$D^+ \to K_S^0 K_S^0 K^+$	$25.4 \pm 0.5 \pm 1.2$	45 ± 20
$D^+ \to K_S^0 K_S^0 \pi^+$	$27.0 \pm 0.5 \pm 1.2$	–
$D^0 \to K_S^0 K_S^0$	$1.67 \pm 0.11 \pm 0.11$	1.7 ± 0.4
$D^0 \to K_S^0 K_S^0 K_S^0$	$7.21 \pm 0.33 \pm 0.44$	9.1 ± 1.3

The maximum change of the reweighted detection efficiencies, 1.0%, is taken as the systematic uncertainty in MC modeling.

Adding all of above systematic uncertainties in quadrature, we obtain the total systematic uncertainties of 4.7%, 4.4%, 6.8% and 6.1% for $D^+ \to K_S^0 K_S^0 K^+$, $D^+ \to K_S^0 K_S^0 \pi^+$, $D^0 \to K_S^0 K_S^0$ and $D^0 \to K_S^0 K_S^0 K_S^0$, respectively.

6. Summary

In summary, by analyzing 2.93 fb^{-1} of data collected at $\sqrt{s} =$ 3.773 GeV with the BESIII detector, we measure the branching fractions for the hadronic decays $D^+ \to K_S^0 K_S^0 K^+$, $D^+ \to K_S^0 K_S^0 \pi^+$, $D^0 \to K_S^0 K_S^0$ and $D^0 \to K_S^0 K_S^0 K_S^0$ using a single-tag method. Table 4 presents the comparisons of the measured branching fractions with the PDG values [1]. The branching fraction for $D^+ \to K_S^0 K_S^0 \pi^+$ is measured for the first time and the others are consistent with previous measurements, but with much improved precision. We also determine the branching fraction ratios $\mathcal{B}(D^+ \to K_S^0 K_S^0 K^+)/\mathcal{B}(D^+ \to K_S^0 K_S^0 \pi^+) = 0.941 \pm 0.025_{\text{stat.}} \pm 0.040_{\text{sys.}}$ and $\mathcal{B}(D^0 \to K_S^0 K_S^0)/\mathcal{B}(D^0 \to K_S^0 K_S^0 K_S^0) = 0.232 \pm 0.019_{\text{stat.}} \pm 0.016_{\text{sys.}}$, in which the systematic uncertainties in the $D^+ D^-$ (or $D^0 \bar{D}^0$) cross section, the integrated luminosity of data, as well as the reconstruction efficiencies and the branching fractions of the two K_S^0 mesons cancel. The results in this analysis provide helpful experimental data to probe for the interplay between the weak and strong interactions in charmed meson decay [2–5]. In addition, the measured branching fraction for the two-body decay $D^0 \to K_S^0 K_S^0$ can also help to understand SU(3)-flavor symmetry breaking effects in D meson decays [6–10].

References

[1] C. Patrignani, et al., Particle Data Group, Chin. Phys. C 40 (2016) 100001.
[2] X.Y. Pham, et al., Phys. Lett. B 193 (1987) 331.
[3] R.E. Karlsen, M.D. Scadron, et al., Phys. Rev. D 45 (1992) 4113.
[4] Y.S. Dai, et al., Phys. Rev. D 60 (1999) 014014.
[5] J.O. Eeg, et al., Phys. Rev. D 64 (2001) 034010.
[6] W. Kwong, S.P. Rosen, Phys. Lett. B 298 (1993) 413.
[7] H.N. Li, et al., Phys. Rev. D 86 (2012) 036012.
[8] Y. Grossman, D.J. Robinson, J. High Energy Phys. 1304 (2013) 67.
[9] S. Müller, et al., Phys. Rev. D 92 (2015) 014004.
[10] A. Biswas, et al., Phys. Rev. D 92 (2015) 014032.
[11] M. Ablikim, et al., BESIII Collaboration, Chin. Phys. C 37 (2013) 123001;
     M. Ablikim, et al., Phys. Lett. B 753 (2016) 629.
[12] M. Ablikim, et al., BESIII Collaboration, Nucl. Instrum. Methods Phys. Res., Sect. A, Accel. Spectrom. Detect. Assoc. Equip. 614 (2010) 345.
[13] H. Albrecht, et al., ARGUS Collaboration, Z. Phys. C 46 (1990) 9.
[14] H. Albrecht, et al., ARGUS Collaboration, Z. Phys. C 64 (1994) 375.
[15] R. Ammar, et al., CLEO Collaboration, Phys. Rev. D 44 (1991) 3383.
[16] D.M. Asner, et al., CLEO Collaboration, Phys. Rev. D 54 (1996) 4211.
[17] J.M. Link, et al., FOCUS Collaboration, Phys. Lett. B 607 (2005) 59.
[18] G. Bonvicini, et al., CLEO Collaboration, Phys. Rev. D 89 (2014) 072002.
[19] S. Agostinelli, et al., GEANT4 Collaboration, Nucl. Instrum. Methods Phys. Res., Sect. A, Accel. Spectrom. Detect. Assoc. Equip. 506 (2003) 250.
[20] S. Jadach, B.F.L. Ward, Z. Was, Comput. Phys. Commun. 130 (2000) 260;
     S. Jadach, B.F.L. Ward, Z. Was, Phys. Rev. D 63 (2001) 113009.
[21] E.A. Kureav, V.S. Fadin, Sov. J. Nucl. Phys. 41 (1985) 466;
     E.A. Kureav, V.S. Fadin, Yad. Fiz. 41 (1985) 733.
[22] E. Richter-Was, Phys. Lett. B 303 (1993) 63.
[23] D.J. Lange, Nucl. Instrum. Methods Phys. Res., Sect. A, Accel. Spectrom. Detect. Assoc. Equip. 462 (2001) 152;
     R.G. Ping, Chin. Phys. C 32 (2008) 599.
[24] J.C. Chen, et al., Phys. Rev. D 62 (2000) 034003.
[25] H. Albrecht, et al., ARGUS Collaboration, Phys. Lett. B 241 (1990) 278.
[26] M. Ablikim, et al., BESIII Collaboration, Phys. Rev. D 92 (2015) 112008.